Computational simulation of biaxial fatigue behaviour of lotus-type porous material

J. Kramberger, M. Šori
University of Maribor, Faculty of mechanical engineering, Smetanova 17, 2000 Maribor, Slovenia
janez.kramberger@um.si
marko.sori@um.si

M. Šraml
University of Maribor, Faculty of civil engineering, transportation engineering and architecture, Smetanova 17, 2000 Maribor, Slovenia
matjaz.sraml@um.si

S. Glodež
University of Maribor, Faculty of mechanical engineering, Smetanova 17, 2000 Maribor, Slovenia
srecko.glodez@um.si

ABSTRACT. A computational simulation of low-cycle fatigue behaviour of lotus-type porous material, subjected to biaxial in-phase loading cycles is presented in this paper. Fatigue properties of porous materials are less frequently published in the literature. This paper evaluates computational analyses, where different pore distribution and biaxial loading conditions in relation to the pore orientations is considered in each simulation. The fatigue analysis is performed by using a damage initiation and evolution law based on the inelastic strain energy. The computational results are subjected to the appropriate statistical analysis, because of different pore topology a different fatigue lives are obtained on the same loading level. Results of computational simulations show also a qualitative understanding of porosity influence on low-cycle fatigue failures of lotus-type porous material under biaxial loading conditions.

KEYWORDS. Lotus-type porous material; Low-cycle fatigue; Damage; Finite element analysis.

INTRODUCTION

P orous materials are relatively new class of materials, which offer potential for lightweight structures, energy absorption and other applications [1-3]. Current manufacturing methods enable to create various porous materials, either open-celled or closed-celled porous structures with varying pore morphology. A new type of porous material with unidirectional cylindrical pores is Lotus-type porous material, which is often used in lightweight structures, medicine, automotive engineering, sports equipment, etc. [4]. The porosity of lotus materials is usually lower than porosity of some conventional porous metals [5].

When porous material is used for a structural component, the fatigue behavior should be taken into account. Some investigations presented in [6-8] cannot be used to describe the fatigue behavior of lotus-type porous materials due to different pore shapes and orientations. The experimental research of the fatigue behavior of copper and magnesium lotus-type porous structures presented by Seki et al [9, 10] has shown that, for the fatigue loading parallel to the longitudinal axis of pores, the stress field in the matrix is homogeneous, and slip bands appear all over the specimen surface. This is not the case for transverse loading, where stress field is inhomogeneous, and slip bands are formed only around pores due to of high stress concentration in this region.

Some existing researches show that the most common method to determine structural properties of porous materials is the experimental investigation [11-14] Determined mechanical property is usually only compressive yield strength or plateau strength while fatigue properties have less frequently been published in details, especially for lotus-type porous materials.

This paper discusses the low-cycle fatigue (LCF) behavior of lotus-type porous material, and evaluates the fatigue damage initiation and propagation through computational simulations using the direct cyclic analysis procedure in the framework of Abaqus/Standard software [15]. It is shown that in displacement controlled regime, cracks are easily detectable via reaction forces.

METHODOLOGY

Computational simulations allow us a better insight into analyzed structure behavior, and can provide information, which is sometimes very difficult or even impossible to determine with experimental measurements. The direct cyclic analysis procedure, implemented in Abaqus/Standard [15], is used in this work to compute the stabilized response of the structure directly, without having to compute a number of sequential cycles that would lead to such a stabilized cycle in the traditional approach. Abaqus/Standard offers a general capability for modelling the progressive damage and failure of ductile materials due to stress reversals and the accumulation of inelastic strain energy when the material is subjected to sub-critical cyclic loadings. Damage initiation and evolution criteria are adopted to determine the low-cycle fatigue damage. These two criteria are based on the stabilized accumulated inelastic hysteresis strain energy per cycle, Δw, as is illustrated in Fig. 1.
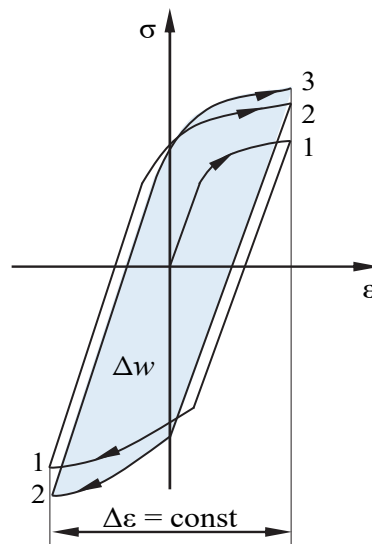

Figure 1: Inelastic hysteresis energy for the stabilized stress cycle

Material failures refer to the complete loss of load-carrying capacity which results from progressive degradation of the material stiffness. The stiffness degradation process is modelled using a damage mechanics theory, which takes into account the process of material degradation due to the initiation, growth and coalescence of micro-cracks/voids in a material element under applied fatigue loading. For low-cycle fatigue analysis, the direct cyclic procedure can be used to directly obtain the stabilized cyclic response of the model. The direct cyclic procedure combines a Fourier series approximation with time integration of the nonlinear material behaviour in order to obtain the stabilized solution iteratively using the modified

Newton method. The number of Fourier terms, the number of iterations and the incrementation during the cyclic time period can be controlled to improve the accuracy [15].

The damage initiation criterion is a phenomenological model for predicting the onset of damage due to stress reversals and the accumulation of inelastic strain in a low-cycle fatigue analysis. It is characterized by the accumulated inelastic hysteresis energy per cycle, Δw, in a material point when the structure response is stabilized in the cycle. The number of stress cycles N_0, corresponding to the damage initiation, is given by [15]:

$$N_0 = c_1 \Delta w^{c2} \tag{1}$$

where $c1$ and $c2$ are material constants. The damage evolution law describes the rate of the material stiffness degradation per cycle once the corresponding damage initiation condition has been reached. For damage in ductile materials, Abaqus/Standard assumes that the degradation of the stiffness can be modelled using a scalar damage variable D where the stress tensor at any given loading cycle during the numerical analysis can be expressed as follows [15]:

$$\sigma = (1 - D)\bar{\sigma} \tag{2}$$

where $\bar{\sigma}$ is the effective (or undamaged) stress tensor that would exist in the material in the absence of damage computed in the current increment. Once the damage criterion is satisfied at the material integration point, the damage state is calculated and updated based on the inelastic hysteresis energy for the stabilized cycle. The rate of damage per cycle is given by:

$$\frac{dD}{dN} = \frac{c_3 \Delta w^{c4}}{L} \tag{3}$$

where $c3$ and $c4$ are material constants, and L is the characteristic length referred to the material point and based on the finite element geometry. It is assumed that material loses its load capacity when D = 1. When this condition is satisfied in a certain finite element, such an element can be removed from the mesh. In such a way, the damage (crack) propagation can be monitored in the proposed computational model.

COMPUTATIONAL MODEL

A general structure of lotus-type porous material is simplified in the computational model and represented by a square with random pore sizes and patterns, as is shown in Fig. 2. The size of the model is 3.3 × 3.3 mm [16]. Five computational models with different pore topologies and the same porosity, equal to 0.234, are generated and examined. The 2D numerical analysis is performed under plane strain loading conditions. All models are discretized with linear plane strain finite elements (CPE4R and CPE3 type of elements). The global size of finite elements 0.03 mm is chosen. The geometric structure, shown in Fig. 2a, is used as a basis for FEM analysis. Fig. 2b shows the applied boundary conditions with bi-axial loading. The load is applied to the top and bottom edge under displacement rate control. The displacement load vary sinusoidal in-phase, in such a way that the global deformation corresponds to values, given by Eq. (4) and (5):

$$\varepsilon_y = \varepsilon_0 \sin(\omega t) \tag{4}$$

$$\gamma_{xy} = (1 + \nu)\varepsilon_0 \sin(\omega t) \tag{5}$$

where ε_0 is a global deformation in y-direction. Selected maximum value of global deformation is ε_0 = 0.1%. The load is applied in the low-cycle fatigue step with a time period of 1 second.

In the numerical analyses, the linear kinematic hardening model with linearized monotonic stress-plastic strain behaviour presented in Tab. 1 is used. Furthermore, the Young's modulus E = 200 GPa and the Poisson's ratio ν = 0.33 is assumed.

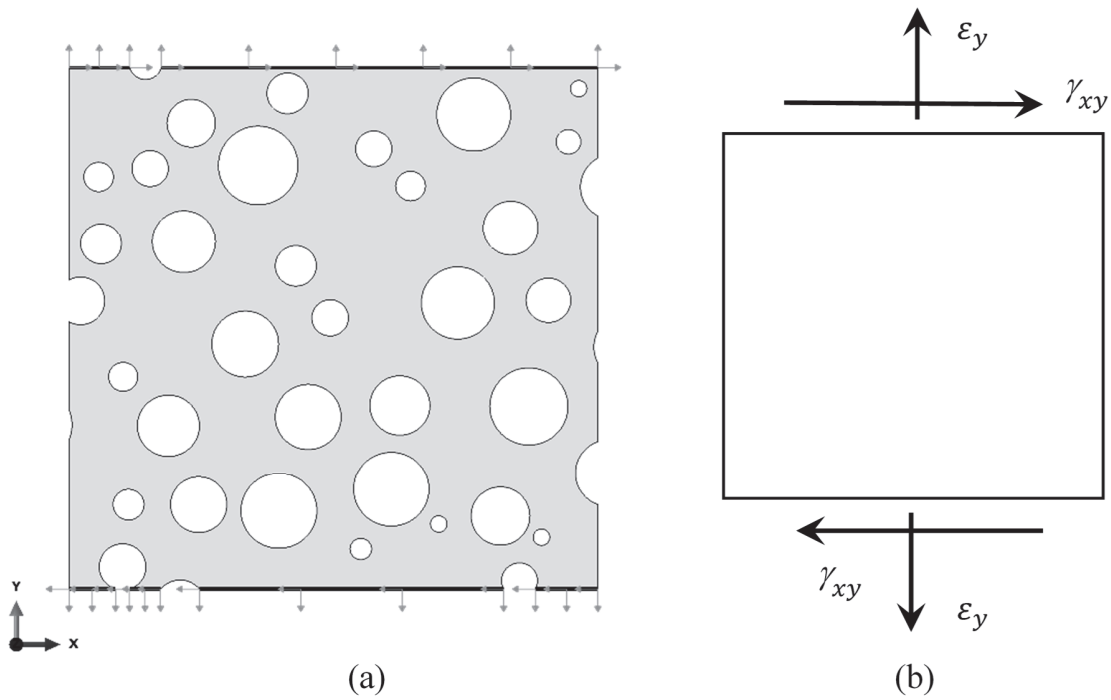Figure 2: (a) Computational model and (b) applied boundary conditions

Stress (MPa)	Plastic strain
400	0
800	24

Table 1: Linearized stress-plastic behavior of the base material [15]

The mechanical properties considered in the damage analysis for the studied porous structure have been obtained from the literature [15]. It should be noted that the values of material parameters c_1 and c_3 in Tab. 2 depend on the system of units in which the model is applied.

$c_1 \left(\dfrac{\text{cycle}}{\text{N}^{c_2}\text{mm}^{-2c_2}} \right)$	c_2	$c_3 \left(\dfrac{\text{cmm}}{\text{cycle}(\text{N}^{c_4}\text{mm}^{-2c_4})} \right)$	c_4
100	24	$2.7 \cdot 10^{-5}$	1.27

Table 2: Material parameters for damage initiation and evolution [15]

RESULTS AND DISCUSSION

Fig. 3 shows the state of all five models at different states through the analysis. After one cycle, there is no damage in any of the models, while after 20 cycles some cracks occur between large adjacent pores.
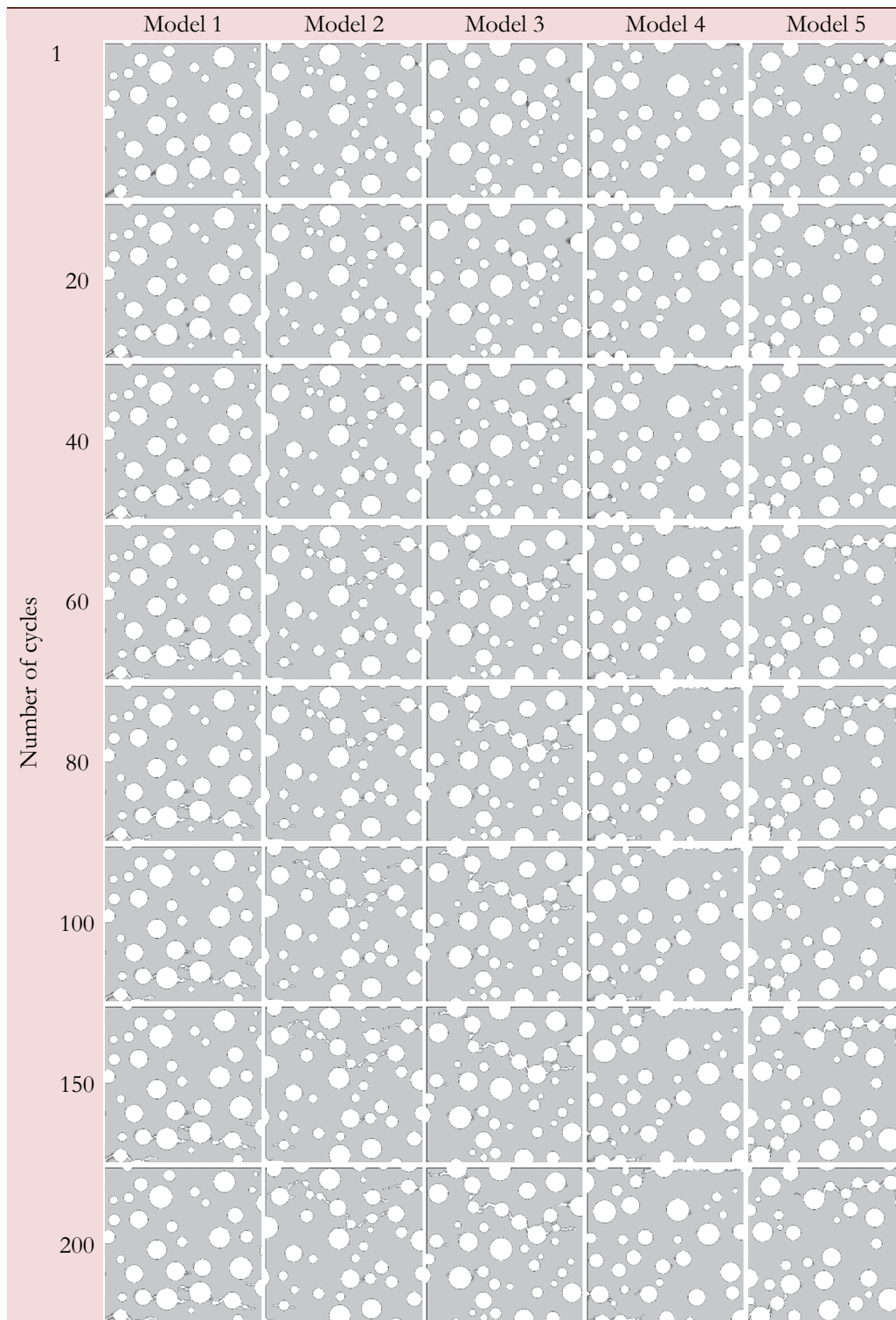
Figure 3: Crack propagation in models with the same porosity and different topology.

After 60 cycles, cracks between the pores and pores themselves form a larger coalesced crack, which is almost completely formed at 100 cycles. Some miniscule crack growth occurs between 100 and 200 cycles, but due to drop of macro-rigidity, the crack growth rate stops near 200 cycles and although the calculation runs until 500 cycles, no further crack growth is detected.

Fig. 4 gives correlation between reaction forces in tension/compression (Y-axis) and shear (X-axis). At the 1st cycle, the magnitude force in tension/compression direction is around 300 N and around 100 N in shear direction. In the first 100 cycles, reaction forces in both directions are dropping linearly, but near zero point, tension/compression component drops to zero, while the shear component remains near 30 N even after 500 cycles – long after crack growth has stopped. Apparently, this is a consequence of local bend-like conditions around the pore, where relatively large pore radius prevents crack initiation.
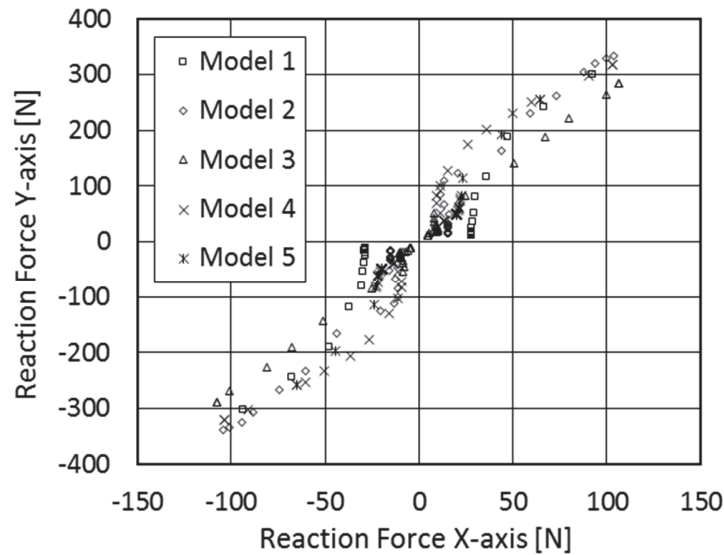

Figure 4: Reaction force shares for different pore morphologies

As seen in Fig. 3, the majority of crack growth occurs in first 100 load cycles, which is also evident from diagram in Fig. 5, where dependence of the reaction force magnitude versus number of load cycles is plotted. There is also some drop between 100 and 200 cycles, but afterwards, reaction force magnitude remains constant. Data even suggests that higher reaction forces at the initiation of damage result lower reaction forces after crack growth, but this fact needs a deeper investigation.
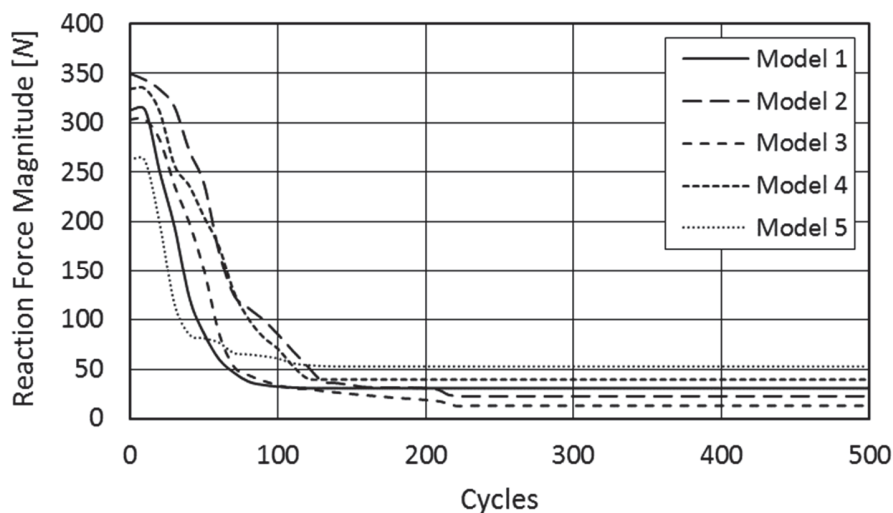

Figure 4: Drop of reaction force magnitude between 1 and 100 cycles

CONCLUSIONS

I n this paper, the response of lotus-type porous material is investigated to biaxial loading that is applied with displacements rate control. It is shown that different pore morphology has some effect on multiaxial LCF-life, but only in form of statistical scatter band. It is shown that adjacent large pores are critical areas for crack formation and growth under given boundary conditions.

Furthermore, it is shown, that with increase of crack length reaction force magnitude decreases towards zero. The tension/compression reaction force drops almost to zero, but shear reaction force remains at 0.3% of the initial shear reaction force. Possible explanation for this phenomenon are local bending-like conditions, which appear near large pores. Large pore radii then serve as stress relaxation areas.

Presented numerical approach for low-cycle multiaxial fatigue failure study based on direct cyclic algorithm and inelastic strain energy is general and efficient. However, further research on modelling other general porous structures will be our tendency in this field.

REFERENCES

[1] Banhart, J., Manufacture, characterisation and application of cellular metals and metal foams, Progress in Materials Science, 46 (2001) 559-632, DOI: 10.1016/S0079-6425(00)00002-5.

[2] Smith, B., Szyniszewski, S., Hajjar, J., Schafer, B., Arwade, S., Steel foam for structures: A review of applications, manufacturing and material properties, Journal of Constructional Steel Research, 71 (2012) 1-10, DOI: 10.1016/j.jcsr.2011.10.028.

[3] Lefebvre, L., Banhart, J., Dunand, D., Porous Metals and Metallic Foams: Current Status and Recent Developments, Advanced Engineering Materials, 10 (2008) 775-787, DOI: 10.1002/adem.200800241.

[4] Vesenjak, M., Kovacic, A., Tane, M., Borovinsek, M., Nakajima, H., Ren, Z., C ompressive properties of lotus-type porous iron, Computational Materials Science, 65 (2012) 37-43, DOI: 10.1016/j.commatsci.2012.07.004.

[5] Seki, H., Tane, M., Nakajima, H., Fatigue crack initiation and propagation in lotus-type porous copper, Materials Transactions, 49 (2008) 144-150, DOI: 10.2320/matertrans.MRA2007623.

[6] Amsterdam, E., De Hosson, J., Onck, P., Failure mechanisms of closed-cell aluminum foam under monotonic and cyclic loading, Acta Materialia, 54 (2006) 4465-4472, DOI: 10.1016/j.actamat.2006.05.033.

[7] Olurin, O., McCullough, K., Fleck, N., Ashby, M., Fatigue crack propagation in aluminium alloy foams, International Journal of Fatigue, 23 (2001) 375-382, DOI: 10.1016/S0142-1123(01)00010-X.

[8] Zhou, J., Gao, Z., Cuitino, A., Soboyejo, W., Effects of heat treatment on the compressive deformation behavior of open cell aluminum foams, Materials Science and Engineering a-Structural Materials Properties Microstructure and Processing, 386 (2004) 118-128, DOI: 10.1016/j.msea.2004.07.042.

[9] Seki, H., Tane, M., Nakajima, H., Effects of anisotropic pore structure and fiber texture on fatigue properties of lotus-type porous magnesium, Journal of Materials Research, 22 (2007) 3120-3129, DOI: 10.1557/JMR.2007.0385.

[10] Seki, H., Tane, M., Otsuka, M., Nakajima, H., Effects of pore morphology on fatigue strength and fracture surface of lotus-type porous copper, Journal of Materials Research, 22 (2007) 1331-1338, DOI: 10.1557/jmr.2007.0164.

[11] Vesenjak, M., Borovinšek, M., Fiedler, T., Higa, Y., Ren, Z., Structural characterisation of advanced pore morphology (APM) foam elements, Materials Letters, 110 (2013) 201-203, DOI: 10.1016/j.matlet.2013.08.026.

[12] Vesenjak, M., Ren, Z., Ochsner, A., Dynamic behaviour of regular closed-cell porous metals – computational study, International Journal of Materials Engineering Innovation, 1 (2009) 175-196, DOI: 10.1504/IJMATEI.2009.029363.

[13] Ingraham, M., DeMaria, C., Issen, K., Morrison, D., Low cycle fatigue of aluminum foam, Materials Science and Engineering a-Structural Materials Properties Microstructure and Processing, 504 (2009) 150-156, DOI: 10.1016/j.msea.2008.10.045

[14] Allison, P.G., Hammi, Y., Jordon, J.B., Horstemeyer, M.F., Modelling and experimental study of fatigue of powder metal steel (FC-0205), Powder Metallurgy, 56 (2014) 388-396, DOI: 10.1179/1743290113Y.0000000063.

[15] Abaqus/CAE User's Manual (ver. 6.12), Dassaults Systemes Inc, 2011.

[16] Kramberger, J., Šraml, M., Glodež, S., Computational study of low-cycle fatigue behaviour of lotus-type porous material, International Journal of Fatigue, In Press (2016), DOI: 10.1016/j.ijfatigue.2016.02.037.